Clouds and cloud radiative forcing over tropical Indian Ocean and their relationship with sea surface temperature

D. S. Pai and M. Rajeevan

India Meteorological Department, Pune 411 005, India

Earth radiation budget experiment (ERBE) radiative fluxes and International Satellite Cloud Climatology Project (ISCCP) C-2 cloud parameters for the four representative months of January, April, July and October and for the period 1985–1988 are used to study the cloud–radiation interaction over the tropical Indian Ocean (20°S–20°N, 50°E–100°E), and its relationship with sea surface temperature (SST). Some important results are compared with those over tropical west Pacific Ocean (20°S–20°N, 130°E–180°E). Over Indian Ocean, both the shortwave cloud radiative forcing (SWCRF) and longwave cloud radiative forcing (LWCRF) are found to be correlated most with high cloud amounts (HCA) among the various cloud types. HCA and cloud radiative forcings in turn show a positive relationship with SST above ~26.4°C. During July and October, after reaching a maximum value at ~29°C, the relationship is found to be negative. In the rising portion of the HCA–SST relationship, at certain SST threshold value (27.4°C for July) the probability of occurrence of high convective clouds suddenly rises above 50%. During January and July above this SST threshold value the SWCRF is found to be significantly larger than LWCRF, thus causing large negative net cloud radiative forcing. This is found to be associated with the sudden rise in the spatial extent (cloud amount) and the optical depth of the high clouds above the SST threshold values.

AT any instant more than half of the earth is cloud-covered. Cloudiness is a pivotal variable for the earth's radiative balance. Clouds also may respond to climate change in such a way as to modulate climate sensitivity significantly. Clouds have two competing effects on earth's energy balance; through the reflection of incoming solar radiation and the trapping of the longwave radiation, leading to cloud greenhouse effect. For understanding the role of clouds in the climate system, cloud radiative forcing is a useful diagnostic. It is also used to validate cloud parameterization employed in General Circulation Models[1,2].

Beginning with the study of Cess[3], there has been a great interest in using satellite data to quantitatively infer the role that clouds play in the climate system. However, the accuracy of most observational results concerning climate scale cloud radiative effects has been diminished by the data available to define clear sky and total sky radiation fields. The Earth radiation budget experiment (ERBE)[4] is the first satellite experiment designed to provide observational data to address this important climatic problem. Ramanathan *et al.*[5] have shown that clouds produce a net cooling of the earth–atmosphere system. Subsequently there have been numerous studies using ERBE data[2,6–10].

Kiehl and Ramanathan[2] showed that over the deep convective regions, there is near-cancellation between longwave cloud radiative forcing and the shortwave cloud radiative forcing. Their study, however, used only one month of ERBE data (i.e. April 1985). But these competing effects of clouds vary with time, space or cloud type and structure. Also the global effects of clouds comprise the average of a large number of regional processes. On regional scale, cloud's behaviour depends on complex dynamic and thermodynamic couplings between the surface and atmosphere[11]. This study is therefore designed to examine the cloud radiative forcing over tropical Indian Ocean (20°S–20°N, 50°E–100°E), and its relationship with the various cloud types and sea surface temperature (SST). Some of the important results are compared with those over tropical west Pacific Ocean (20°S–20°N, 130°E–180°E). We have also used relatively larger data set than Kiehl and Ramanathan[2].

We have examined the relationship of cloud radiative forcings with different cloud types as well as discussed the variation of high cloud amounts with SST. We have also analysed the variation of SWCRF with respect to LWCRF, and demonstrated that, over tropical Indian Ocean, the balance between SWCRF and LWCRF does not exist with large high clouds.

One of the data sets employed in this study is longwave and shortwave radiative fluxes at the top of the atmosphere (TOA) from the ERBE. The data include the fluxes under both all sky as well as clear sky conditions gridded at a 2.5° × 2.5°, lat. × lon. resolution. Cloud radiative forcing is defined as the influence of clouds on the input of radiative energy to the earth–atmosphere system at the TOA[5]. Its variation represents the feedback of clouds on the climate system. The net radiative heating, H, for the entire surface to atmosphere column of a cloudy domain is

$$H = S(1 - A) - F, \tag{1}$$

where S is the solar irradiance, A is the albedo and F is the longwave flux emitted to space. If H_{clr} is the clear sky net heating, then the net cloud radiative forcing (net CRF) is given as:

$$\text{Net CRF} = H - H_{clr}. \tag{2}$$

If the domain has no clouds, $H = H_{clr}$ and net CRF = 0.

From equation (1), the net radiative heating H is the difference between absorbed solar radiation $S(1-A)$ and emitted longwave flux F at TOA.

Therefore from eqs (1) and (2) we can write net CRF as the sum of the shortwave cloud radiative forcing (SWCRF) and longwave cloud radiative forcing (LWCRF), i.e.

Net CRF = SWCRF + LWCRF,

where SWCRF = $S(A_{clr} - A)$, and LWCRF = $F_{clr} - F$; A_{clr} is the clear sky albedo and F_{clr} is the clear sky longwave radiation flux at TOA. When clouds are present, they reflect more solar energy into space than would clear skies. SWCRF gives a quantitative estimate of this effect. SWCRF is typically negative and describes the difference between the clear sky and cloudy sky reflected solar fluxes at TOA. LWCRF measures the decrease of thermal energy into the space radiated by the atmosphere column due to the presence of clouds. It is typically a positive quantity.

In the ERBE data there are few grid boxes with missing clear sky fluxes. In order to calculate the cloud radiative forcings, these missing clear sky fluxes have to be filled. This is achieved by filling these missing grid boxes with the mean of the clear sky fluxes at the nearest grid boxes[10]. Since the clear sky fluxes over the oceans are relatively uniform on small scales, the errors resulting from the filling are expected to be small. Moreover, the number of the missing grid boxes was very small compared to the total number of grid boxes.

International Satellite Cloud Climatology Project (ISCCP) cloud parameters are based on observations by the global network of geostationary weather satellites and at least one polar-orbiting NOAA satellite. The measurements utilized in this study are taken from the ISCCP C-2 data set[12]. These are monthly averages of various cloud parameters on the same $2.5° \times 2.5°$ grid used by ERBE. We have mainly used two cloud parameters, cloud amounts and optical thickness. Clouds are mainly divided into three types: High clouds (cirrus, cirrostratus/cirrocumulus and convective clouds) have cloud tops above the pressure levels of 440 hpa level; Middle clouds (nimbostratus and altocumulus/altostratus) have cloud tops located between the pressure levels of 440 hpa and 680 hpa; Low clouds (stratus and cumulus/stratocumulus) have tops below the 680 hpa level, near the typical height of the tropical trade cumulus boundary-layer top.

The SST data is taken from the monthly analysis of National Centre for Environmental Prediction (NCEP), USA, which is derived from ship, buoy and satellite measurements[13]. This data set provides monthly mean SST on a $2° \times 2°$ spatial grid. We interpolated these values to overlap into $2.5° \times 2.5°$ grids of ERBE and ISCCP data.

For each year during the period 1985–1988, we have used the above-described data for the four representative months of January, April, July and October. ERBE data for 1985 January is not available, and, therefore in all, we have considered 15 months for this study. To get a composite picture of the relationships we have combined all the grid box values coming under the same months. As a result, there are four cases corresponding to the four representative months of January, April, July and October.

To examine the relationship between cloud radiative forcing with macrophysical properties of clouds, we have correlated the cloud radiative forcing with low, middle, high and total cloud amounts. The square of the correlation coefficients for LWCRF and SWCRF with various cloud types over tropical Indian Ocean is given in Table 1. Both the SWCRF and LWCRF are correlated most with the high cloud amounts (HCA) during all the months. It means that high clouds contribute significantly to both greenhouse trapping as well as reflection of solar radiation. The observed relationship between LWCRF and HCA is obvious as the LWCRF is primarily determined by the difference between the surface and the cloud top temperatures. It is also important to note that the correlation of LWCRF and SWCRF with HCA was larger than that with the total cloud amount.

The relationship between SWCRF and HCA may be explained as due to the fact that the cloud albedo increases with the increase in the areal extent and the optical depth of the high clouds[14]. This is, in fact, associated with the increase in the SSTs. Figure 1 shows mean optical depths for 0.4°C SST bins plotted as a function of SST (°C) for the tropical Indian Ocean for the months of January, April, July and October. In all the months, the optical depths of both the type of high clouds (cirrus and cirrostratus) in general increase with SST. The cloud albedo of high clouds depend on the scattering behaviour of individual ice particles, integrated over both the particle size distribution and the path length through the cloud. As the SST increases, production of colder cirrus clouds, spreading thousands of kilometres downwind, may contain smaller ice particles due to the fallout of the larger particles with increasing distance downwind of the convective towers. The ice particles of reduced effective radii are more efficient in reflecting short wave radiation relative to long wave absorption. This enhancement in the short wave reflection is in addition to that caused by the increase in cirrus ice mass alone.

In general, LWCRF and SWCRF have no significant relationship with low cloud amounts (LCA) except during July when it is moderate. This may be associated with the natural bias of satellite observation to upper level clouds. It is difficult to diagnose low clouds change because they cannot be detected by satellite visible and infra-red radiometers on the scale of a satellite pixel if they are underneath of higher clouds[15]. Using ISCCP C-2 data, Fu *et al.*[11] analysed fractional contributions of different cloud types to the total

Table 1. Square of the correlation coefficients for ERBE, LWCRF and SWCRF against ISCCP low, middle, high and total cloud amount

		Cloud type							
		Low		Medium		High		Total	
Month	Year	LWCRF	SWCRF	LWCRF	SWCRF	LWCRF	SWCRF	LWCRF	SWCRF
January	1985								
	1986	0.12	0.07	0.47	0.38	0.95	0.90	0.63	0.65
	1987	0.23	0.17	0.74	0.67	0.95	0.91	0.66	0.68
	1988	0.13	0.05	0.63	0.54	0.96	0.87	0.67	0.70
April	1985	0.06	0.04	0.74	0.66	0.93	0.88	0.62	0.61
	1986	0.00	0.00	0.36	0.31	0.83	0.79	0.38	0.35
	1987	0.00	0.00	0.71	0.70	0.90	0.90	0.64	0.64
	1988	0.05	0.05	0.56	0.58	0.91	0.85	0.41	0.39
July	1985	0.66	0.50	0.22	0.15	0.91	0.73	0.44	0.45
	1986	0.65	0.55	0.34	0.18	0.94	0.80	0.38	0.35
	1987	0.52	0.41	0.52	0.38	0.94	0.84	0.46	0.49
	1988	0.80	0.70	0.13	0.07	0.93	0.84	0.50	0.50
October	1985	0.51	0.31	0.59	0.62	0.95	0.80	0.60	0.68
	1986	0.30	0.19	0.69	0.65	0.97	0.89	0.70	0.73
	1987	0.56	0.43	0.56	0.50	0.95	0.86	0.56	0.58
	1988	0.27	0.12	0.69	0.48	0.95	0.76	0.67	0.63

cloudiness for annual mean climatology, and found that over tropical Indian Ocean, high clouds contribute major part of the total cloud variations. In this region, the upper level clouds mainly occur in association with deep convective activity in the inter-tropical convergence zone (ITCZ). Whenever the low clouds happen to exist under the high or middle clouds, some of the low clouds may not be seen by satellite radiometers. Also, the changes of high and middle clouds may create a spurious change in the low cloud field. For example, in a region where the high clouds are relatively frequent when the high or middle clouds decrease, satellite radiometers may see low clouds which were previously overshadowed by high or middle clouds and indicate a spurious increase of low clouds. Over the tropical west Pacific Ocean, the sign and magnitude of the correlation coefficients between cloud radiative forcings and cloud types (data not shown) is in the same order as that over Indian Ocean.

To examine the relationship between HCA, which is a proxy for deep convection, and SST over tropical Indian Ocean, we have plotted means and standard deviations of HCA for 0.4°C SST bins against SST for all the four months (Figure 2). The dashed curves represent the probability of grid points having ≥ 20% HCA expressed as percentage for each SST bin. HCA and outgoing long-wave radiation (OLR) has reciprocal relationship and HCA of 20% is approximately equal to OLR of 240 Wm^{-2}. It is well known that regions with OLR of ≤ 240 Wm^{-2} represent deep convective regions[16]. The solid curves connecting the mean HCA indicate that in general HCA and therefore the organized convection increases as SSTs increase from around 26.4°C and reaches a maximum between 28.8°C and 30.4°C. During July and October, the HCA after reaching its maximum value around 29°C decreases with increasing SST. Optical depths of cirrus clouds also exhibit a similar variation (Figure 1). Along the rising portion of the curve we define an SST threshold as one at which the probability of grid points with more than 20% HCA reach 50% or more. This threshold value of SST is similar to the one suggested by Gadgil *et al.*[17] who analysed monthly index for cloudiness intensity associated with large-scale convection during the monsoon season over the north Indian Ocean. The threshold SST value represents the approximate large-scale surface temperature required to provide necessary moist static energy to the near surface layer in order for saturated air parcels to ascend into the high troposphere and for deep convection to occur. During July this threshold SST is 27.6°C. Similarly for January, April and October the threshold SST values are 28.0°C, 29.6°C and 27.6°C respectively. However, it may be mentioned that except during the month of July, there are a number of grid points with no high clouds even though SST is above the threshold value. These results demonstrate clearly that higher local SST is necessary but not sufficient condition for deep convection. Even though a warmer SST increases the buoyancy of the air in the planetary boundary layer, if this buoyancy is suppressed by factors like subsidence, or a stable stratified boundary layer, deep convection and thus high clouds will not be promoted.

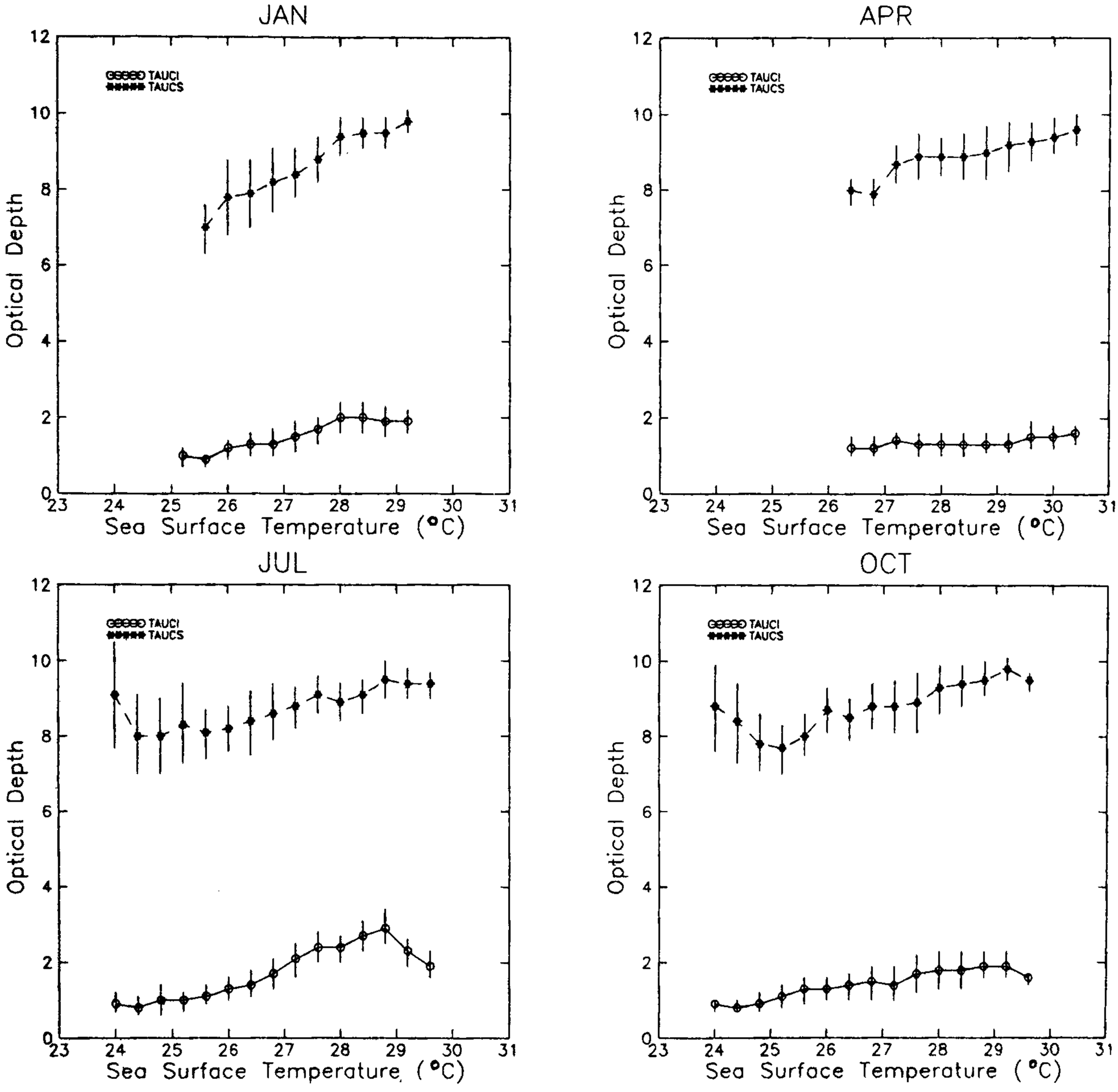

Figure 1. Variation of mean monthly ISCCP visible optical depths for cirrus (TAUCI) and cirrostratus (TAUCS) for 0.4°C SST bins as a function of SST (°C) for the tropical Indian Ocean for the months of January, April, July and October. Vertical bars are standard deviations of the means. The solid (dashed) curve connects the mean optical depths of cirrus (cirrostratus) clouds.

The decreasing portion of the relationship at warmer SSTs, during July and October, can be associated to diminished deep convection. These may be the regions where local large-scale circulation patterns or remote forcings are acting to suppress deep convection. Waliser and Graham[18] addressed this important aspect in which they emphasize the importance of cooling mechanisms associated with deep convection in determining the observed upper limits on tropical SST. We have noticed that grid boxes with such depressed convection over warm SST regions are mainly observed over the Arabian Sea and western parts of the equatorial Indian Ocean. This depressed convective activity may be associated with the presence of low-level thermal inversion over this region. Sen and Das[19] using data from summer monsoon experiment (MONEX-79) have reported the presence of thermal inversion in the lower levels over the Arabian sea during summer monsoon period. The formation of inversion was attributed mainly to the confluence of the dry warm air of continental origin and the relatively cool moist air of oceanic origin. Low-level inversions over Arabian Sea were present even during the established phase of the southwest monsoon. Even if the SSTs are conducive, such low-level inversions may

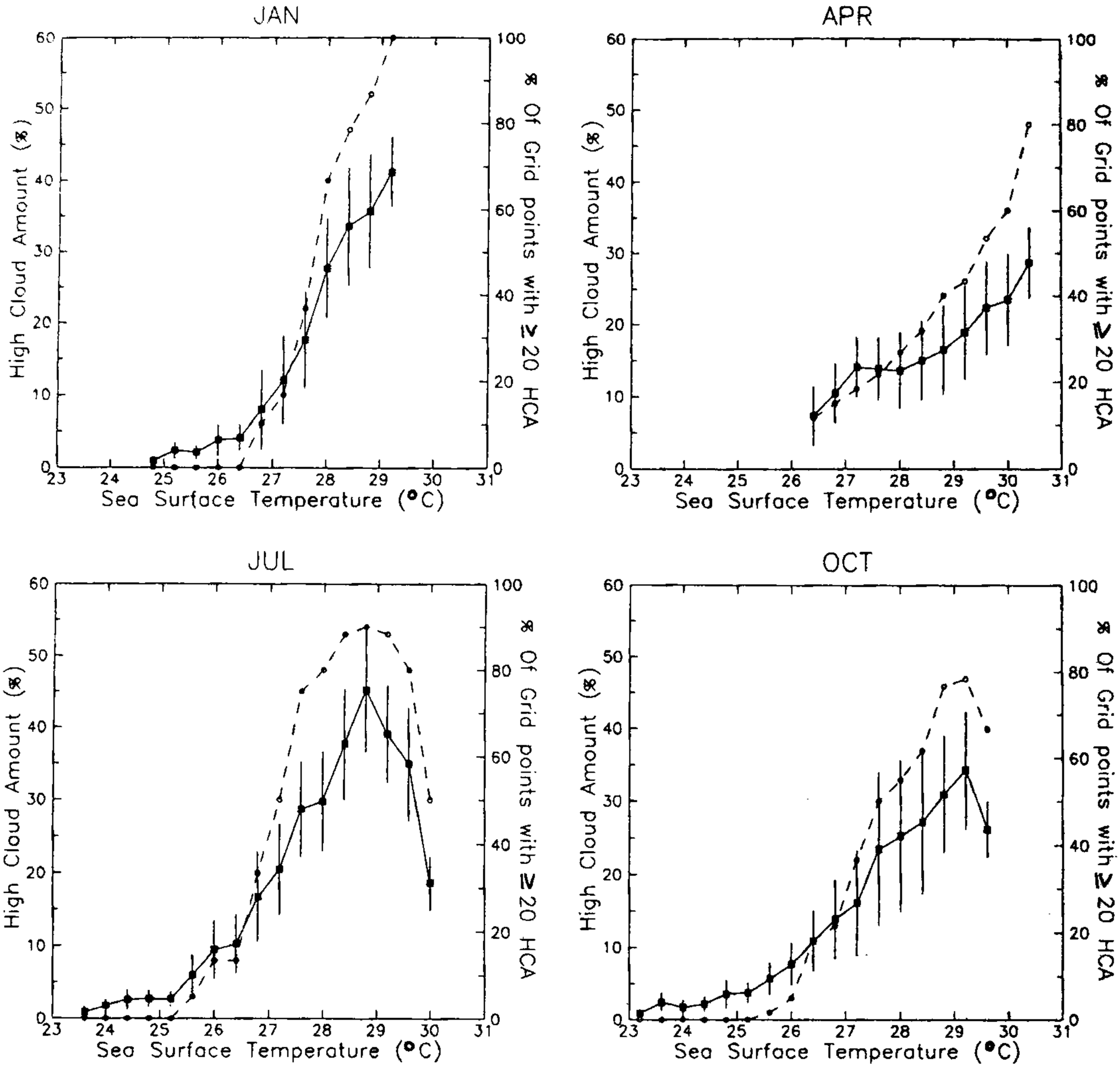

Figure 2. Variation of mean monthly ISCCP HCA (%) for 0.4°C SST bins as function of SST (°C) for the tropical Indian Ocean for the months of January, April, July and October. Vertical bars are standard deviations of the means. The solid curve connects the means. The dashed curves connect the probability of occurrence of grid points with ≥ 20% HCA expressed in percentage for each 0.4°C SST bins.

inhibit active organized convection. Srinivasan[16] highlights the crucial role played by the energy available in the troposphere on the diminished deep convective activity over the regions where SSTs are otherwise favourable for the active deep convection. He observed that for the existence of deep convective activity the net energy covergence in the troposphere should be positive.

Figure 3 shows the HCA–SST relationship for tropical west Pacific Ocean. The main features of this relationship are similar to those discussed for Indian Ocean. Above ~24°C HCA increases with SST. The threshold SST values for January, April, July and October are 28.8°C , 28.8°C, 28.4°C and 29.2°C respectively. However the major difference is in the months showing decreasing portion of the HCA–SST relationship. For example, over tropical Indian Ocean decreasing portion of the HCA–SST relationship (Figure 2) is observed during July and October (note that these are monsoon months) only. Whereas, over the tropical west Pacific Occean this is observed in January and April. During January and April after reaching its maximum value at ~29.6°C, HCA decreases with SST.

Kiehl and Ramanathan[2] showed that over deep convective Indonesian region, there is near-cancellation between the SWCRF and the LWCRF. To examine

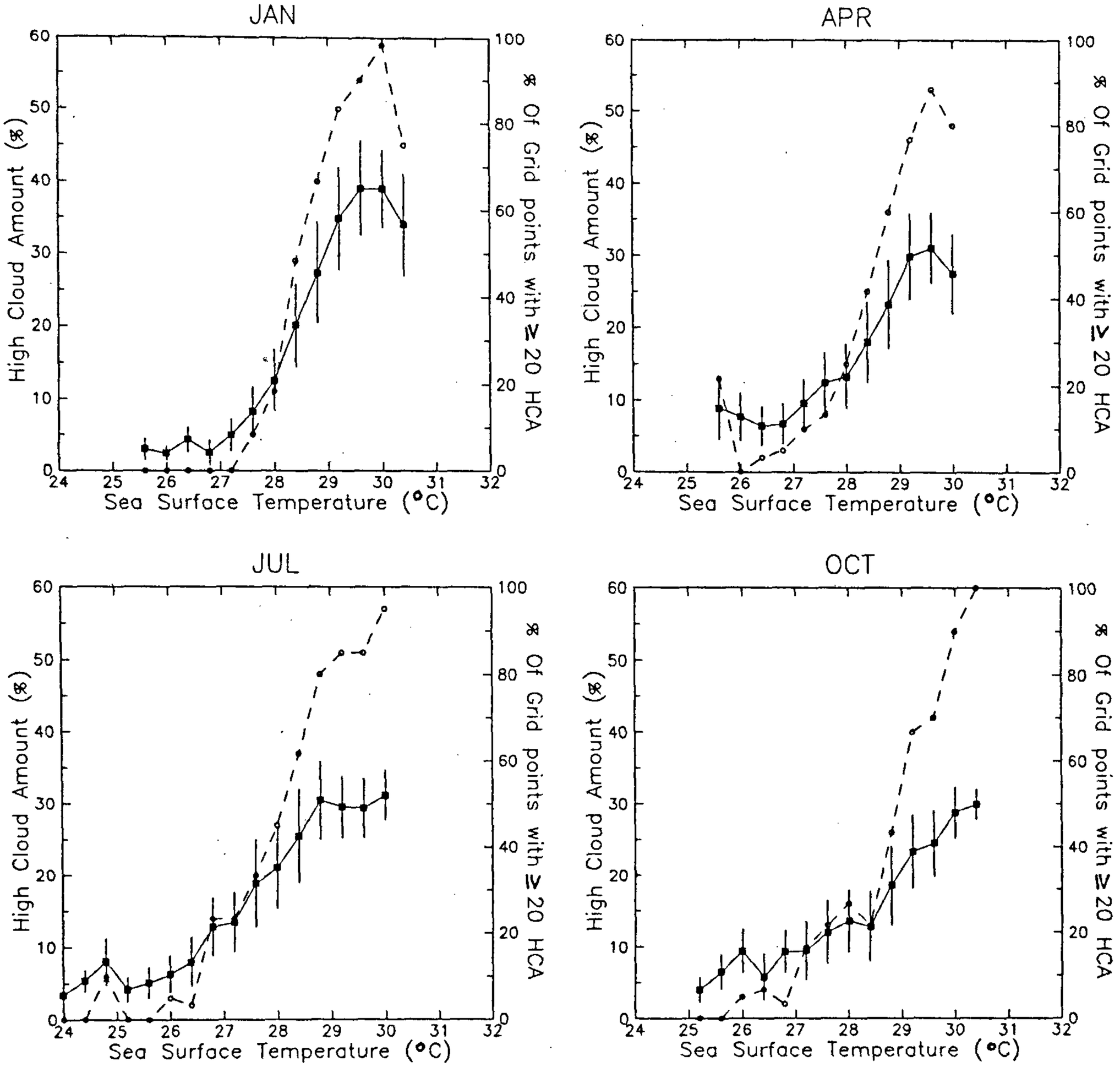

Figure 3. Variation of mean monthly ISCCP HCA (%) for 0.4°C SST bins as function of SST (°C) for the tropical west Pacific Ocean for the months of January, April, July and October. Vertical bars are standard deviations of the means. The solid curve connects the means. The dashed curves connect the probability of occurrence of grid points with ≥ 20% HCA expressed in percentage for each 0.4°C SST bins.

whether such near-cancellation is observed over tropical Indian Ocean, we have plotted grid box values of SWCRF against that of LWCRF for four representative months of January, April, July and October. The results are shown in Figure 4. The diagonal solid line in each diagram represents the points where SWCRF and LWCRF exactly cancel each other. The two dotted lines on either side of the solid line are shifted by ±10 Wm^{-2} which represents the estimated uncertainty in the regional estimates of the net cloud radiative forcing, using ERBE data. Near-cancellation between SWCRF and LWCRF is more closely observed during the month of April in which most of the data points lie between the two dotted lines of ±10 Wm^{-2} uncertainty. During the other three months, more points lie below the solid line, which implies that negative SWCRF is slightly more than the positive LWCRF. There are many data points which are even outside the −10 Wm^{-2} dotted line, which again implies SWCRF is comparatively larger in magnitude. Particularly in July the differences are very large.

Figure 5 shows the relationship of SWCRF, LWCRF and net CRF with SST over tropical Indian Ocean. The grid box values of cloud radiative forcing are pooled into 0.4°C SST bins. The standard deviations are plotted

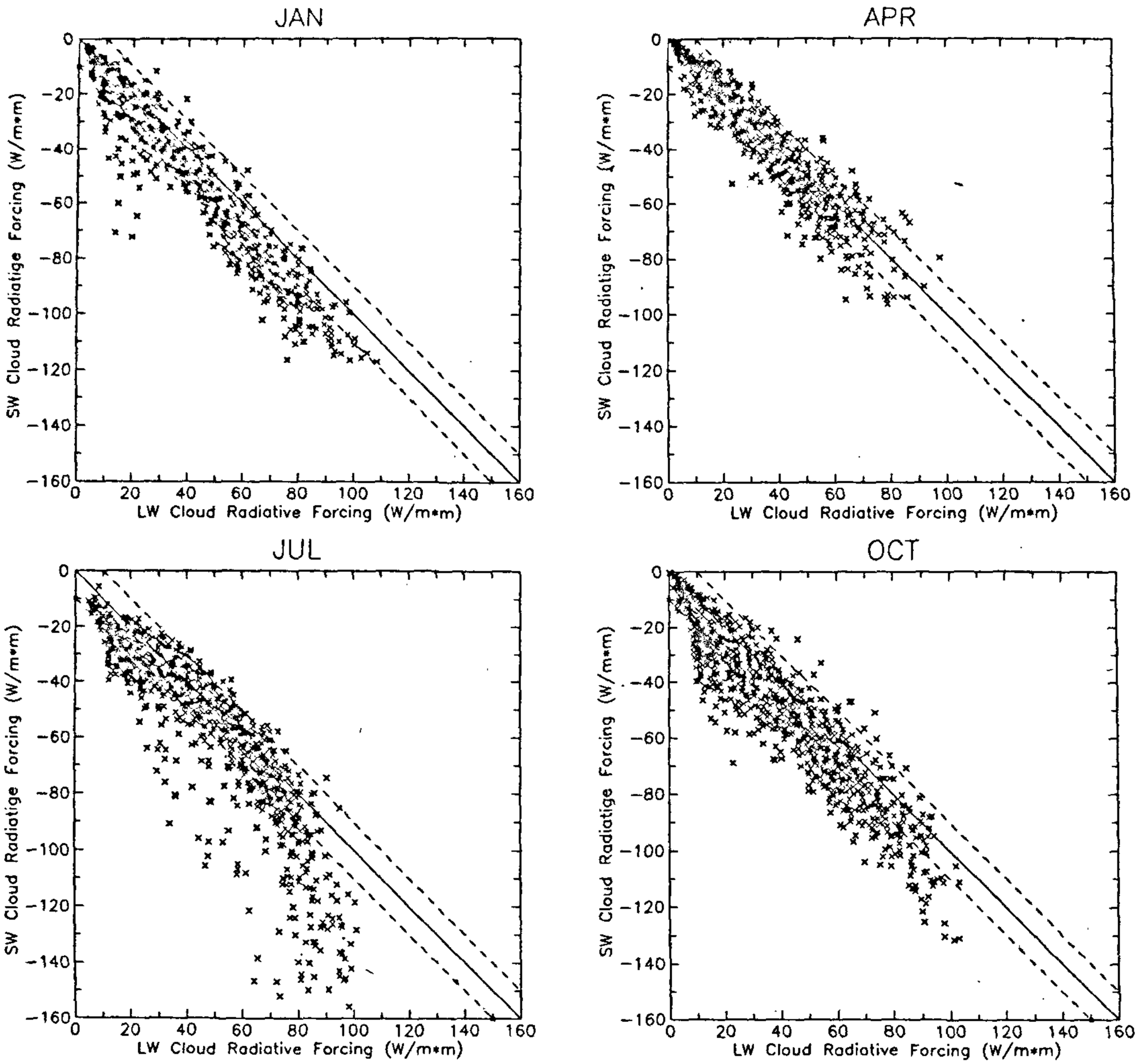

Figure 4. Monthly earth radiation budget experiment (ERBE) LWCRF versus SWCRF (Wm^{-2}) for the tropical Indian Ocean. Each point represents a grid value within the region for the months of January, April, July and October. The dotted lines indicate $\pm$ 10 Wm^{-2}.

as vertical bars. In general, the relationships of LWCRF and SWCRF with SST is almost similar to that of optical depth (Figure 1) and HCA (Figure 2) with SST. During July and October, two discontinuities, one at 26.4°C and other at 29°C, are clearly observed. These types of discontinuities are also noticed in the relationship between SST and large-scale vertical motions[20]. During April, for all SST regions the cancellation between LWCRF and SWCRF is very near as evident by the location of mean net CRF curve within the horizontal dotted lines of $\pm$10 W/m^{-2}. During January, the absence of cancellation of CRFs is mainly concentrated in the SST region of > 28°C. In about 50% of the grid points with SST greater than 28°C, SWCRF is larger than LWCRF by more than 10 Wm^{-2}. During July, there are two regions of SST where absence of cancellation of CRFs is observed. One is below 26.4°C and the other is around 28.8°C. In the first region there are about 50% grid points where SWCRF exceeds LWCRF by more than 10 Wm^{-2}, and in the second region there are about 45% such grid points. During October, the lack of cancellation is mainly limited to regions of SST less than 26.4°C with about 70% grid points where SWCRF exceeds LWCRF by 10 Wm^{-2}. Therefore absence of cancellation between LWCRF and SWCRF is observed during January, July and October, and both over cold SST

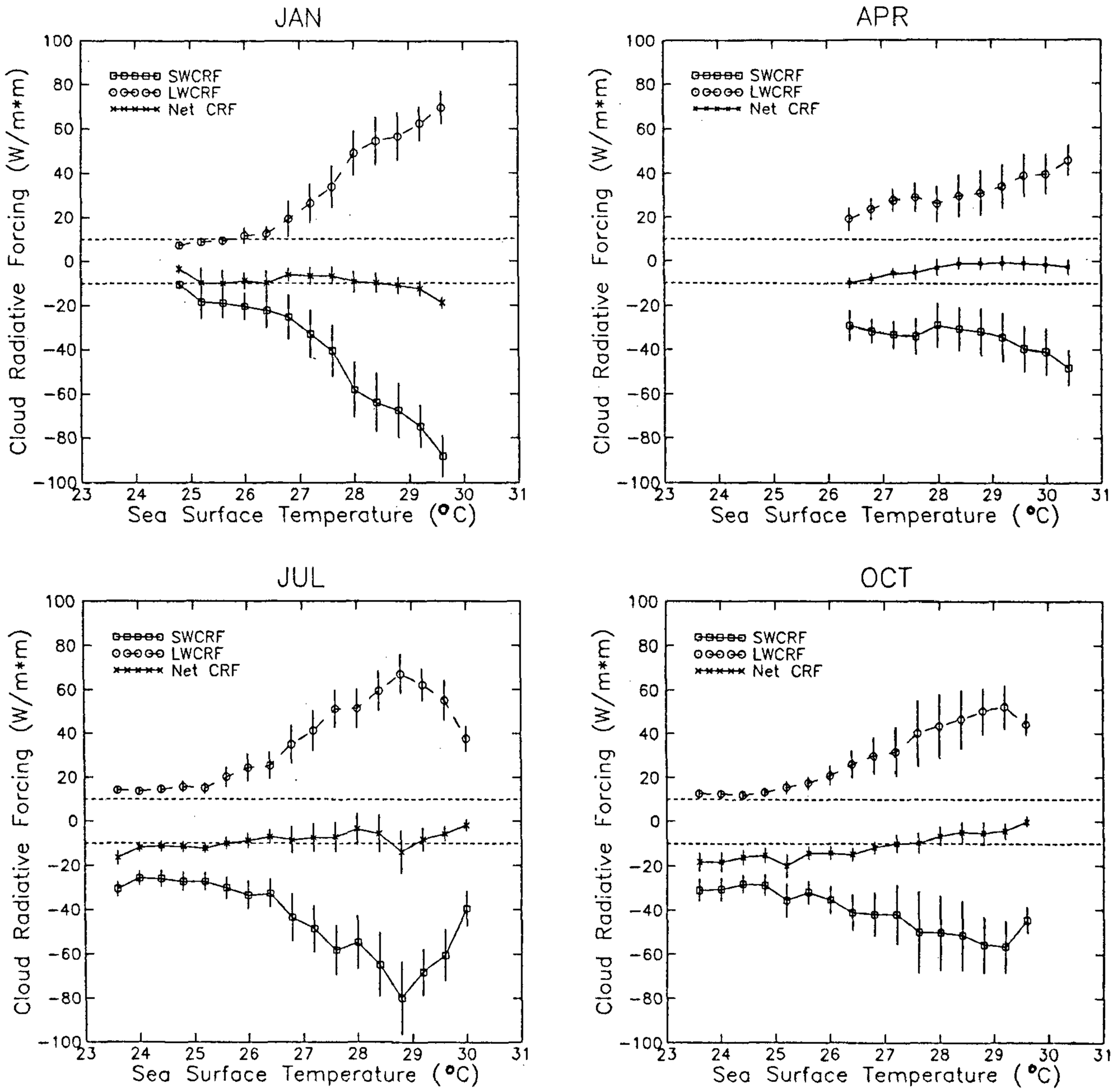

Figure 5. Relationship of SWCRF, LWCRF and net CRF (Wm^{-2}) for 0.4°C SST bins as a function of SST (°C) for the tropical Indian Ocean for the months of January, April, July and October. Vertical bars are standard deviations of the means. The dotted lines indicate $\pm$ 10 Wm^{-2}.

(≤ 26.4°C) regions as well as warm SST (around and above the SST threshold values) regions. Such absence of near-cancellation between SWCRF and LWCRF have implications on cloud radiative feedback on surface temperature[21]. Over colder SST regions, this may be due to the highly reflecting low clouds and fogs.

The absence of near-cancellation between SWCRF and LWCRF over regions with warmer SST is associated with larger HCA as evident in Figure 6. The solid (dotted) curve indicates a plot of mean net CRF for equal intervals (5%) HCA for tropical Indian Ocean (west Pacific). Vertical bars are standard deviations of the means. It is observed that over Indian Ocean during January, above 30% HCA the mean negative net CRF exceeds 10 Wm^{-2}. In about 70% of the grid points with HCA of 30% or more, negative net CRF exceeds 10 Wm^{-2}. On the other hand, during July and October, regions with HCA of ≥ 50% showed negative net CRF exceeding 10 Wm^{-2}. The mean net CRF in this region is of the order of about -30 Wm^{-2}. Also in about 75% of the grid points with 50% or more HCA, negative net CRF exceeded 10 Wm^{-2}. During April, this imbalance is not clearly observed. Therefore, in general, we can conclude that when HCA increases above 30% in January,

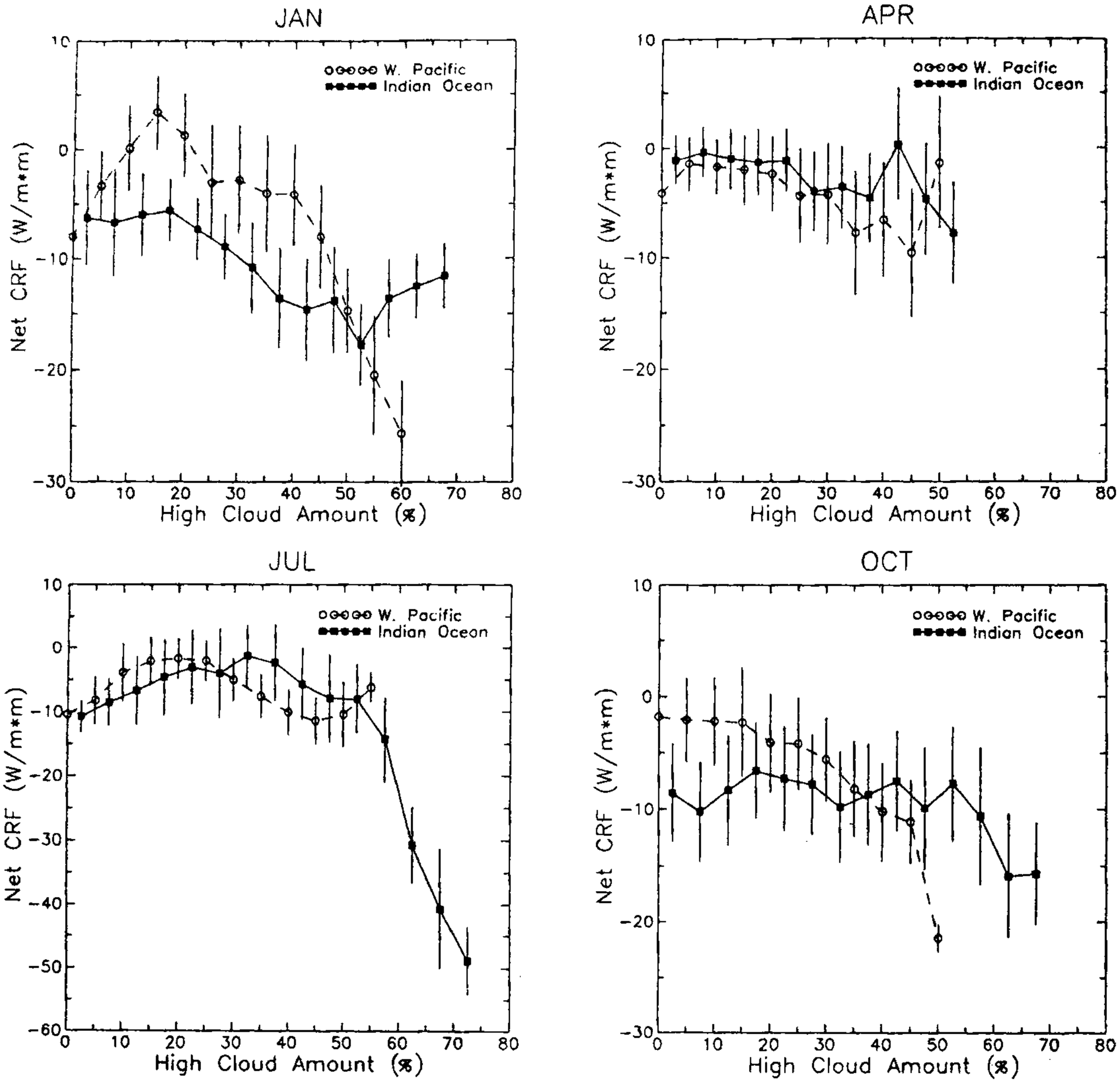

Figure 6. Variation of mean monthly ERBE net CRF (Wm^{-2}) for 5% HCA bins as a function of HCA (%) for the months of January, April, July and October. Vertical bars are standard deviations of the means. The solid (dashed) curve connects the means over tropical Indian Ocean (West Pacific).

and 50% in July and October, there is a tendency of imbalance between SWCRF and LWCRF.

Over tropical west Pacific Ocean, during January when HCA is $\geq 45\%$, the mean negative net CRF exceeds 10 W/m^{-2} and ~80% of the grid points show negative net CRF ≥ 10 W/m^{-2}. During October, when HCA increases above 40% the mean negative net CRF exceeds 10 W/m^{-2}, and 50% of the grid points show negative net CRF ≥ 10 W/m^{-2}. However during April and July, imbalance between SWCRF and LWCRF is not observed at high HCA. These results show that irrespective of the ocean basins, the imbalance between SWCRF and LWCRF is possible at large HCA.

In order to know the quantitative difference between the CRFs over the tropical Indian Ocean as a single unit, we computed the monthly area averaged SWCRF and LWCRF for all 15 months used in this study. It was found that except during the April months, the differences between the magnitudes of the area averaged CRFs are large and negative. During some months these differences are significant (-10 Wm^{-2}), for example in July 1988 this was ~ -15 Wm^{-2}.

From the above discussions we can obtain the following conclusions:

(1) In addition to the spatial extent (both vertical and horizontal) of the high clouds, its albedo also increases with SST. As a result, HCA was found to influence the LWCRF and SWCRF more than the other cloud types.

(2) Over tropical Indian Ocean at SSTs above 26.4°C, the HCA and the components of CRF increase linearly with SST, and at certain SST threshold (~27.6°C during July). When the probability of occurrence of deep convective activity becomes > 50%, this increase becomes very rapid. This feature is observed over tropical Pacific Ocean also. However this increase with SST does not always sustain at very warm SSTs. Over tropical Indian (west Pacific) Ocean during July and October (January and April) due to the suppressed deep convection at SSTs above ~29°C (29.6°C) the HCA and the components of CRF are found to decrease with increasing SST.

(3) In general, during April, there is a near-cancellation between LWCRF and SWCRF over the tropical Indian Ocean. During October, over lower SST (26.4°C) and during January and July months mainly over warm SST (above and around the SST threshold values) regions, the SWCRF is found to be greater than LWCRF, resulting in the lack of cancellation between LWCRF and SWCRF. Except in April months the differences between area weighted monthly SWCRF and LWCRF over tropical Indian Ocean are significantly large and negative.

(4) Over tropical Indian (west Pacific) Ocean during January and July (January and October) when HCA becomes very large (~40–50%), the cloud albedo seems to increase much faster than the longwave absorption, resulting in net cloud radiative cooling of the region by the clouds.

But we would like to put a word of caution to these results particularly of January and July because of seasonal changes in the incoming solar radiation and the solar zenith angle, both of which have complex and largely unknown effects on the cloud forcings.

1. Cess, R. D. *et al.*, *J. Geophys. Res.*, 1996, **101**, 12791–12794.
2. Kiehl, J. T. and Ramanathan, V., *J. Geophys. Res.*, 1990, **95**, 11679–11698.
3. Cess, R. D., *J. Atmos. Sci.*, 1976, **33**, 1831–1843.
4. Barkstrom, B. R., *Bull. Am. Meteorol. Soc.*, 1984, **65**, 1170–1185.
5. Ramanathan, V., Cess, R. R., Harrison, E. F., Minnis, P., Barkstrom, B. R., Ahmad, E. and Hartmann, D., *Science*, 1989, **243**, 57–63.
6. Raval, A. and Ramanathan, V., *Nature*, 1989, **342**, 758–761.
7. Harrison, J. S., Minnis, P., Barkstrom, B. R., Ramanathan, V., Cess, R. D. and Gibson, G. G., *J. Geophys. Res.*, 1990, **95**, 18687–18703.
8. Kiehl, J. T., *J. Climate*, 1994, **7**, 559–565.
9. Zhang, M. H., Cess, R. D., Kwon, T. Y. and Chen, M. H., *J. Geophys. Res.*, 1994, **99**, 5515–5523.
10. Zhang, M. H., Cess, R. D. and Xie, S. C., *J. Climate*, 1996, **9**, 1374–1384.
11. Fu, R., Liu, W. T. and Dickinson, R. E., *J. Climate*, 1996, **9**, 616–634.
12. Rossow, W. B. and Schiffer, R. A., *Bull. Am. Meteorol. Soc.*, 1991, **72**, 2–20.
13. Reynolds, R. W., *J. Climate*, 1988, **1**, 75–88.
14. Heymsfield, A. J. and Miloshevich, L. M., *Nature*, 1991, **351**, 14–15.
15. Rossow, W. B. and Lacis, A. A., *J. Climate*, 1990, **3**, 1240–1253.
16. Srinivasan, J., *J. Indian Inst. Sci.*, 1997, **77**, 237–255.
17. Gadgil, S. P., Joseph, P. V. and Joshi, N. V., *Nature*, 1984, **312**, 141–143.
18. Waliser, D. E. and Graham, N. E., *J. Geophys. Res.*, 1993, **98**, 12881–12893.
19. Sen, P. N. and Das, H. P., *Mausam*, 1986, **37**, 117–122.
20. Bony, S., Lau, K. M. and Sud, Y. C., *J. Climate*, 1997, **10**, 2055–2077.
21. Ramanathan, V. and Collins, W., *Nature*, 1991, **351**, 27–32.

ACKNOWLEDGEMENTS. We are grateful to DGM, India Meteorological Department for permitting us to submit the paper to this journal, to Dr U. S. De for his encouragement and useful suggestions and to Dr S. K. Dikshit for his encouragement and for providing facilities to carry out this research work. Our sincere thanks are also due to Prof. J. Srinivasan for going through this manuscript and for giving very useful suggestions. The data sets used in this study were obtained from the NASA Langley Research Center EOSDIS Distributed Active Archive Center. M.R. thanks NASA for supplying these data sets. We also thank the anonymous referees for their valuable suggestions.

Received 24 November 1997; revised accepted 9 June 1998

Toxicity of *tuibur*, a unique form of tobacco smoke extract used in Mizoram, India

J. Mahanta*, M. Chetia, N. C. Hazarika, K. Narain and S. K. Sharma

Regional Medical Research Centre (North Eastern region), Indian Council of Medical Research, Post Box 105, Dibrugarh 786 001, India

A unique form of water extract of tobacco smoke called *tuibur* is used by some people in Mizoram. The toxicity of tuibur was studied using modified version of *Allium* test. Even dilute solutions of *tuibur* exhibited significant toxicity by reducing the root growth of *Allium* bulbs and inducing tumour formation in the roots. Microscopical features revealed reduction of mitotic index, formation of micronuclei, lagging chromosome and c-mitosis in the root tip cells treated with different concentrations of *tuibur*. EC_{50} value of *tuibur* for root growth was also estimated.

TOBACCO use by people is an ancient practice, probably started in the early 1400s. It is estimated that the use of tobacco kills about three million people globally every

*For correspondence